IN-SITU STRENGTH MEASUREMENT BY REAL TIME MONITORING OF TRANSVERSE CRACKS

T.A. Sebaey*, N. Blanco, J. Costa

AMADE, Polytechnic School, Universitat de Girona, Campus Montilivi s/n, 17071 Girona, Spain.

Key words: Transverse Cracking; Strength; Laminate mechanics; Optical Microscopy.

Summary. *Failure of a ply due to transverse loading is one of the mechanisms accounted for in physically-based failure criteria, used in composites design. Experimental data, however, is scarce and the measurement techniques used in the past are time consuming and involve lot of specimen handling during testing. Some physical information is currently well consolidated (such as the dependence of the strength on ply thickness, or in-situ strength) but relevant open questions remain. This work presents a methodology, which does not interfere with the tensile test, to detect transverse cracks by optical means. Four different configurations of CFRP are considered. The results show that there is a dependence of the in-situ strength on the ply thickness and the orientation of the adjacent layers. In the case of thick transverse plies, the strength is controlled by transverse cracks whereas, in thin plies, longitudinal ply splitting occurs before transverse matrix cracking.*

1. Introduction

The popularity of laminated composites in the aerospace and aircraft industries raises the need to have reliable and accurate simulation techniques. The accuracy of the simulations depends on the correct definition of material properties. One of the terms that determines the onset of damage in the progressive failure analysis of laminated composites is the *in-situ* strength [1–4], which can be defined as the strength of the ply taking into account its thickness, position in the whole laminate and the stiffness of the adjacent plies.

To measure the transverse *in-situ* strength, the specimen must be designed to have 90° ply at the middle of the laminate surrounded by plies of other orientations at the surface. It is worth remarking that, few published experimental works were focused on measuring the transverse tensile strength of an embedded ply ([5, 6] for carbon/epoxy and [7] for glass/epoxy). Moreover, the use of these available results for the validation of *in-situ* strength criteria and/or damage models is limited by the lack of a complete set of material properties.

This paper aims to study the effect on the *in-situ* transverse tensile strength of an embedded 90° ply of the ply thickness and of the stiffness of the neighboring plies, by means of a new technique to measure the crack density with respect to the applied mechanical strain. Neither unloading nor handling the specimen for inspection are required. In order to obtain the *in-situ* strength from the experimental data, the procedure summarized in [5], which is based on the Classical Lamination Theory (CLT), is used. Four ply sequences are tested ($[\pm 45/90_n]_s$ (n = 1, 2 and 4) and $[0_2/90_4]_s$). With this focused test campaign, it has been possible to assess the usefulness of the devised methodology to monitor ply matrix cracking, while delivering results that are not accounted for in the current *in-situ* strength criteria.

2. Experiments

The material used in this study was a carbon/epoxy material, Hexcel M21/T800, widely used in aeronautic structures. The pre-impregnated plies were laid in the desired configuration and cured according to the Hexcel's specifications. After curing in an autoclave at 180°C, the specimens were cut into the final dimensions using a diamond disk. The unidirectional elastic properties and strengths were measured according to the corresponding ASTM standards, Table 2. . The thermal and fracture properties were taken from the literature [8].

Elastic properties	E_1 = 130.7 GPa; E_2 = 8.01 GPa; G_{12} = 3.95 GPa; ν_{12} = 0.35
Strength	Y^T = 40.5 MPa; S^L = 69.6 MPa
Thermal Properties	α_1 = 2.1 $\mu\varepsilon$/°C; α_2 = 24 $\mu\varepsilon$/°C
Fracture properties	G_{Ic} = 250 J/m^2; G_{IIc} = 500 J/m^2
Nominal ply thickness	0.184 mm

Table 1. M21/T800 carbon/epoxy unidirectional properties

Four symmetric and balanced stacking sequences were selected; $[\pm 45/90]_s$, $[\pm 45/90_2]_s$, $[\pm 45/90_4]_s$ and $[0_2/90_4]_s$. The first, the second and the third laminates were used to check the effect of the thickness of the 90° layer with the same adjacent layers (±45°). The third and the fourth were used to check the effect of the orientation of the adjacent layers for the same 90° layer thickness. The specimens were 180 mm long and 30 mm wide. The thickness was dependant on the stacking sequence.

The specimen was loaded by means of an universal testing machine (MTS INSIGHT100) with a 100 KN load cell. The longitudinal strain was measured using an axial extensometer (MTS 634.25 F-24) with a gage length of 50 mm and 50% maximum extension. An 18 Megapixel Canon digital camera (EOS 550D) with macro lenses (100 mm f/2.8 Macro L IS USM) were used to monitor 40 mm of the specimen edge (the middle of the zone between the grips). Special care was taken to focus properly on both extremes, top and bottom, of the field of view. With the aid of the camera's SDK (Software Development Kit), connected via a USB port to a PC, it was possible to take a picture every 5 seconds. The test setup is shown in Fig. 1.

The specimen was loaded at 1.0 mm/min. During loading, the camera took a picture every 5 seconds. The process continued, uninterrupted, until the final failure of the specimen (neither stop nor unloading was required). The image acquisition was synchronized with the reading of the load and the strain from the testing machine, so each image could be easily attributed to the load and strain on the specimen at the moment where the picture was taken.

The methodology adopted to calculate the *in-situ* tensile strength is that used by Flaggs and Kural [5]. Based on the Classical Lamination Theory in a symmetrical laminate, the mechanical strain in the global coordinate system (ε_i) can be calculated as a function of the applied mechanical load (P) and the membrane stiffness matrix A_{ij} ($\varepsilon_i = A_{ij}^{-1} P_j$). By transformation ($\varepsilon_i^k = T_{ij}^k \varepsilon_j$) the mechanical strain in the local coordinate system can be calculated for each layer k.

The thermal induced stress due to the curing process should be estimated based on the difference between the room temperature (T_r) and the stress free temperature (T_{sf}). This stress is highly

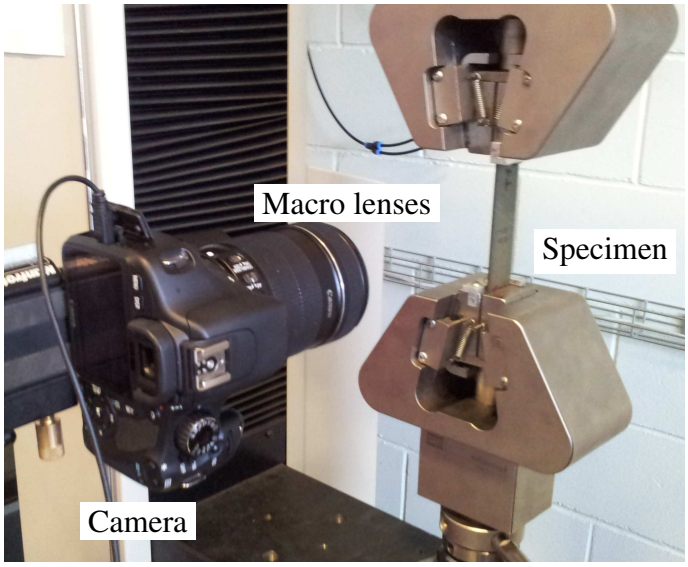

Figure 1. Transverse tensile test setup

dependent on the curing temperature [9, 10]. At curing temperature, the laminate can not be considered as stress free due to the existence of chemical residual stresses. The value of T_{sf} is usually 15°C higher than the curing temperature [11]. Through the current analysis, the value of 195°C was used as T_{sf} and, consequently, the value of ΔT was -172°C ($\Delta T = T_r - T_{sf}$ where T_r = 23°C).

3. Results and discussions

To illustrate the outcome of the experimental methodology described above, Fig. 2 and **??** show some of the sequences of pictures obtained for the configurations $[\pm 45/90_4]_s$. Matrix cracks can be easily detected on the images. The configuration $[\pm 45/90_2]_s$ behaves in the same manner as the configuration $[\pm 45/90_4]_s$. A different response is observed in the images obtained for $[\pm 45/90]_s$. The transverse crack openings are too small to be observed in the reduced resolution. However, in the full resolution, the cracks are clearly identifiable.

The crack density versus the applied strain for the entire test campaign can be shown in Fig. 3. Good repeatability is obtained for each configuration. It is worth remarking that the data in Fig. 3 is limited to the data taken before the appearance of the longitudinal ply splitting. The response is perfectly linear until a certain limit [12]. The slope of the linear part is dependant on the relative stiffness between the 90° layer and the neighboring layers [13].

Relevant information that can be inferred from this experiment is the stiffness degradation in terms of the crack density, [14, 15]. Then, Fig. 4 shows the evolution of the secant modulus of the laminates as a function of the applied strain for one specimen of each configuration. The strain, at which the first transverse crack is observed, is indicated with $\uparrow$ whereas the initiation of ply splitting is marked with $\Uparrow$. There is good agreement between the strains at where these damage phenomena were first observed and the change of slope of the stiffness curves.

Before observing transverse cracks, the configuration $[0_2/90_4]_s$, Fig. 4(d), shows a constant

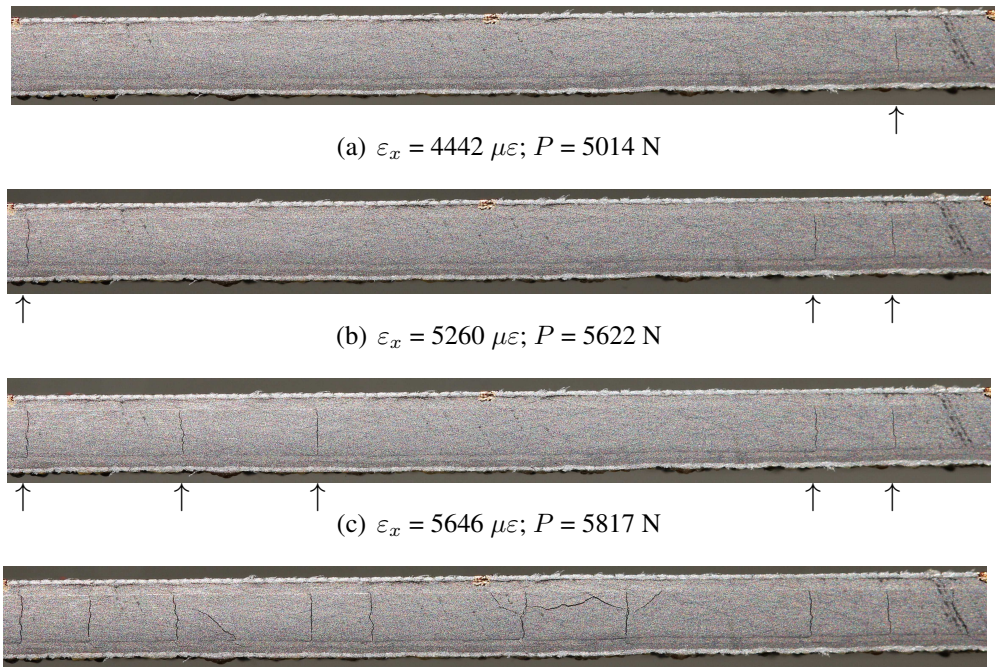

(a) ε_x = 4442 $\mu\varepsilon$; P = 5014 N

(b) ε_x = 5260 $\mu\varepsilon$; P = 5622 N

(c) ε_x = 5646 $\mu\varepsilon$; P = 5817 N

(d) At saturation; ε_x = 7947 $\mu\varepsilon$; P = 7210 N

Figure 2. Sequence of pictures obtained for $[\pm 45/90_4]_s$ and the corresponding data (Crack position is marked with ↑)

stiffness whereas for the specimens with ± 45 as outer layers ($[\pm 45/90_n]_s$) the stiffness curve is constant until a threshold strain from where the stiffness decreases. The same trend is recognized in the in-plane shear test of $[\pm 45]_{16}$. The coincidence of the strain at which the stiffness starts to decay supports this idea. Similar results are shown in [16] for $[\pm 45/90_4]_s$ glass/epoxy laminates.

For the configurations $[\pm 45/90_2]_s$ (Fig. 4(b)), $[\pm 45/90_4]_s$ (Fig. 4(c)) and $[0_2/90_4]_s$ (Fig. 4(d)), the slope of the stiffness curve changes at the initiation of transverse cracks and the reduction continues with a constant slope until the appearance of ply splitting. The configuration $[\pm 45/90]_s$ shows a different trend, Fig. 4(a): the onset and accumulation of observed transverse cracks do not alter the decay rate of the stiffness. The onset of ply splitting causes a relevant change of the slope of the curve. This behavior of the $[\pm 45/90]_s$ reveals that these transverse cracks are only free edge cracks i.e. they do not propagate through the full specimen width. This result is in agreement with the observation of Parvizi et al. [7] for glass/epoxy laminates with thin transverse plies.

Based on this analysis, the transverse tensile strength of the configurations $[\pm 45/90_2]_s$,$[\pm 45/90_4]_s$ and $[0_2/90_4]_s$ is taken as the stress for the onset of transverse cracks. This stress derives from the critical strain, which is calculated by means of a linear fitting of the crack density versus applied strain, Fig. 3. The critical strain corresponds to the extrapolation of the fitting line to zero crack density.

Taking into account that the observed transverse cracks for the configuration $[\pm 45/90]_s$, do not have an influence on the mechanical behavior of the laminate as they are only free edge cracks, the tensile strength is taken as the onset of ply splitting. Then, for $[\pm 45/90]_s$, the strain level

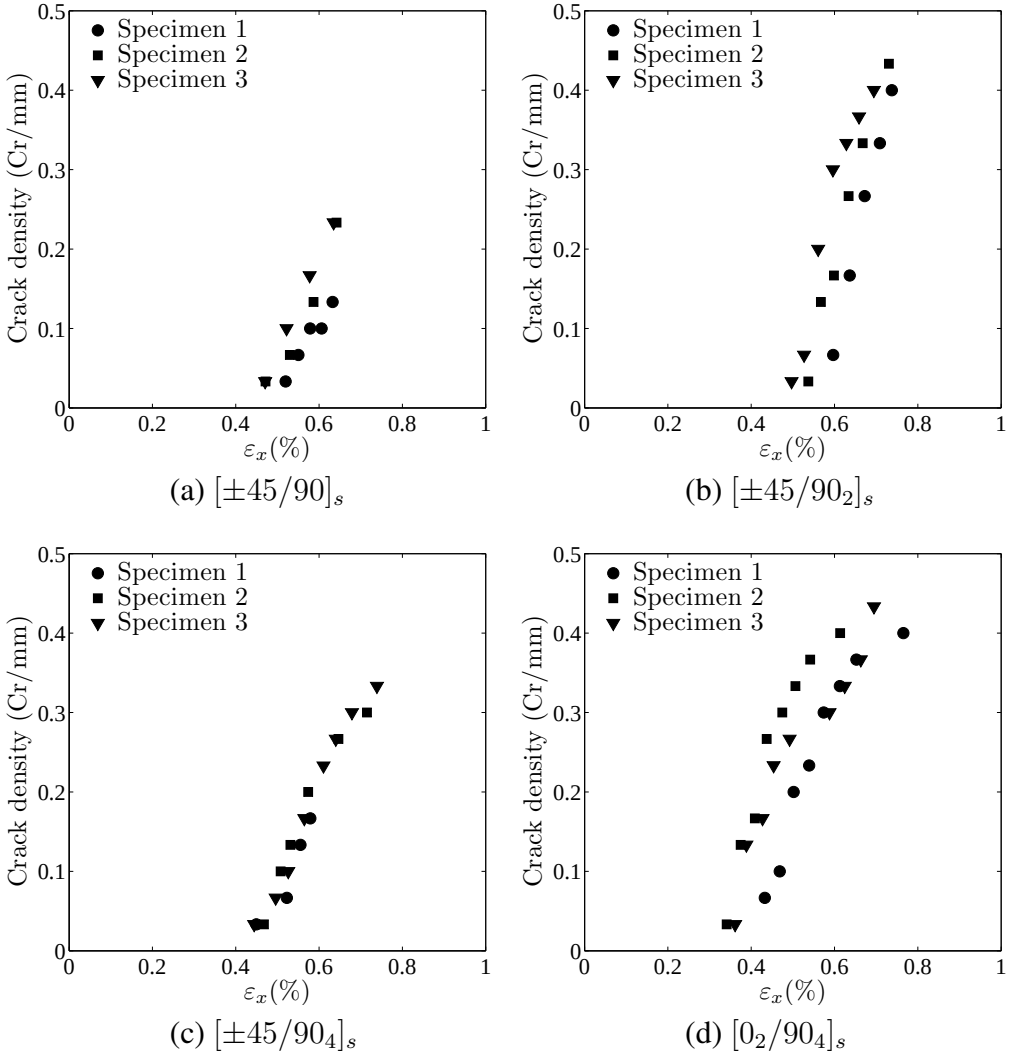

(a) $[\pm 45/90]_s$ (b) $[\pm 45/90_2]_s$

(c) $[\pm 45/90_4]_s$ (d) $[0_2/90_4]_s$

Figure 3. Crack density vs. strain

corresponding to the ply splitting (the strain level marked with ⇑ in Fig. 4) is considered as the critical strain. In spite of the fact of being a different micromechanism from that considered for the other laminates, this definition is useful for design. Between these two competing failure mechanisms (transverse cracking and ply splitting) ply splitting is that which appears at lower stress in $[\pm 45/90]_s$.

In Fig. 5, the measured values of the transverse tensile *in-situ* strength are compared to those predicted using a physically-based *in-situ* model [1, 3, 4]. However, this approach does not take into account the effect of neighboring plies.

The comparison between the configurations $[0_2/90_4]_s$ and $[\pm 45/90_4]_s$ shows that the *in-situ* strength of the first is 10% higher than that of the second. This means that the stiffness of the neighboring plies does have an effect on the strength of the transverse ply. This result is in agreement with the phenomenological proposal of Wang and Karihaloo [17]. However, the available physically-based *in-situ* model, Eq. (**??**) and (**??**) does not account for this effect.

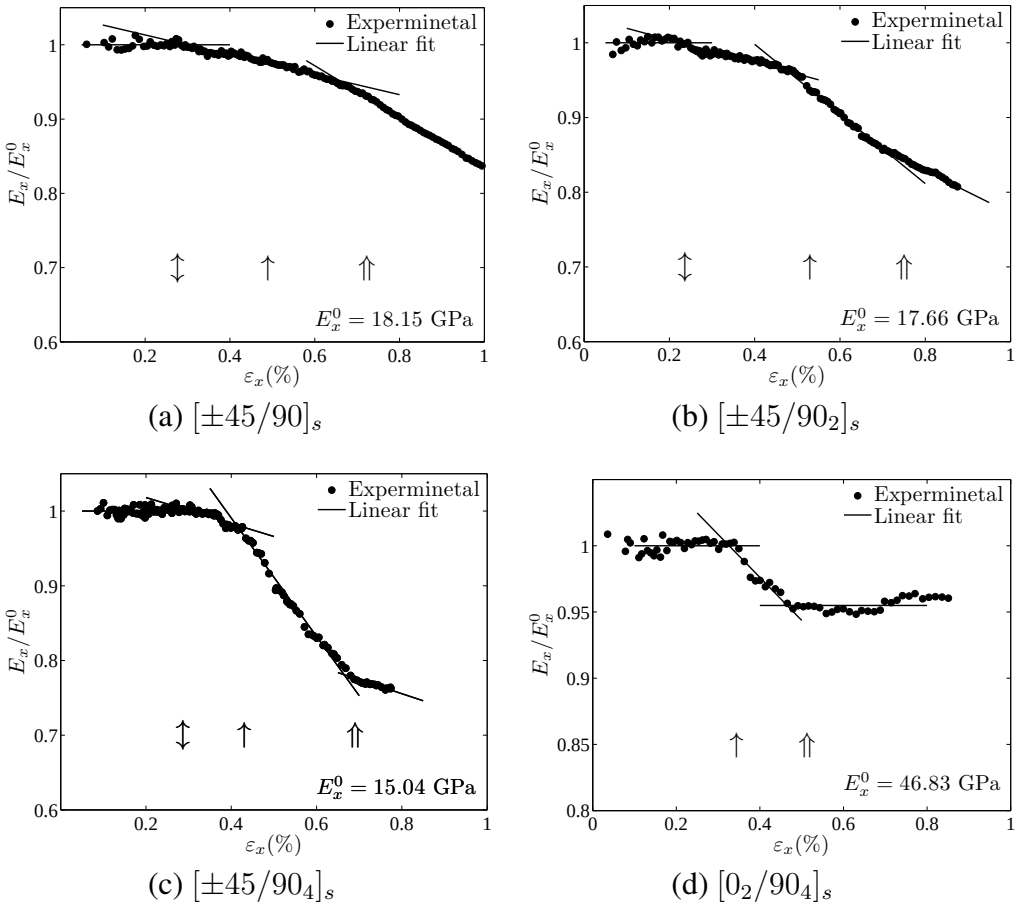

(a) $[\pm 45/90]_s$ (b) $[\pm 45/90_2]_s$

(c) $[\pm 45/90_4]_s$ (d) $[0_2/90_4]_s$

Figure 4. Stiffness vs. the applied strain ($\updownarrow$ represents the initiation of ± 45 nonlinearity, $\uparrow$ defines the initiation of transverse cracking and $\Uparrow$ defines the initiation of ply splitting).

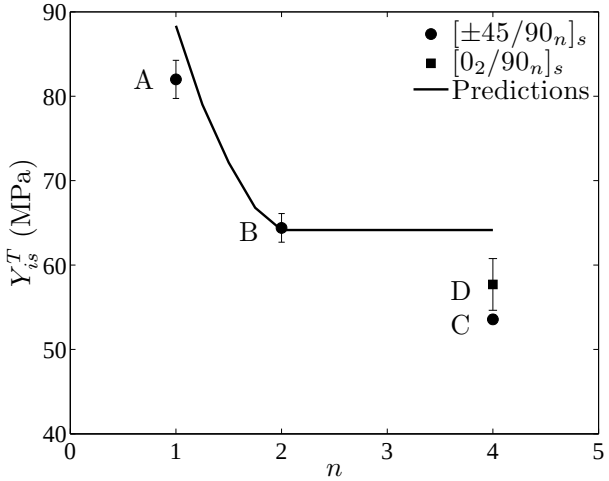

Figure 5. *In-situ* strength as a function of the ply thickness (Point A corresponds to longitudinal ply splitting whereas B, C and D correspond to transverse cracking).

These results show the usefulness of the prescribed methodology to measure the *in-situ* strength based on the real time monitoring of microcracks and the stiffness degradation. A thorough test

campaign over $[\pm\theta/90_n]_s$ laminates of properly characterized material would provide the necessary background to assess the predictive capability of existing *in-situ* models or to introduce the appropriate refinements to them.

4. Conclusions

Four stacking sequences were used to measure the *in-situ* transverse tensile strength of 90° plies surrounded by 0° or ±45° layers. A new methodology based on the *real time* image acquisition of the specimen edge was presented to detect cracking in the transverse layers without interrupting, unloading or handling the specimen for inspection. The Classical Lamination Theory was used to calculate the *in-situ* strength.

The observed damage mechanisms were first transverse plies, and then longitudinal ply splitting. The observed cracks in thin transverse plies did not have an influence on the specimen stiffness as they were only free edge cracks. Thus, the longitudinal splitting was considered as the mechanisms determining the ply strength in this case. On the other hand, in thick transverse plies, the transverse cracks controlled the ply strength. The measured values of the *in-situ* transverse tensile strength exhibited a dependency on the stiffness of neighboring plies as well as on the thickness of the transverse layers.

References

[1] Camanho P.P., Dávila C.G., Pinho S.T., Iannucci L., Robinson P. Prediction of in situ strengths and matrix cracking in composites under transverse tension and in-plane shear. *Composites: Part A*, **37**, pp. 165–176 (2006).

[2] Camanho P.P., Lambert M. A design methodology for mechanically fastened joints in laminated composite materials. *Composites Science and Technology*, **66**, pp. 3004–3020 (2006).

[3] Dávila C.G., Camanho P.P. Failure criteria for FRP laminates in plane stress. Technical Report NASA/TM-2003-212663, NASA, Langley, Research Center, Hampton, November (2003).

[4] Pinho S.T., Dávila C.G., Camanho P.P, IannucciL., Robinson P. Failure models and criteria for FRP under in-plane or three-dimensional stress states including shear non-linearity. Technical Report NASA/TM-2005-213530, NASA, Langley, Research Center, Hampton, February (2005).

[5] Flaggs D.L., Kural M.H. Experimental determination of the in situ transverse lamina strength in graphite/epoxy laminates. *Journal of Composite Materials*, **16**, pp. 103–116 (1982).

[6] Bailey J.E., Curtis P.T., Parvizi A. Transverse cracking and longitudinal splitting behaviour of glass and carbon fibre reinforced epoxy cross ply laminates and the effect of poisson and thermally generatedstrain. In *Proceedings of the Royal Society of London. Series* A*, Mathematical and Physical Sciences*, 366, pp. 599–623 (1979).

[7] Parvizi A., Garrett K.W., Bailey J.E. Constrained cracking in glass fibre-reinforced epoxy cross-ply laminates. *Journal of Materials Science*, **13**, pp. 195–201 (1978).

[8] Zhang X., Boscolo M., Figueroa-Gordon D., Allegri G., Irving P. E.. Fail-safe design of integral metallic aircraft structures reinforced by bonded crack retarders. *Engineering Fracture Mechanics*, **76**, pp. 114–133 (2009).

[9] Gigliotti M., Wisnom M.R., Potter K.D. Development of curvature during the cure of AS4/8552 [0/90] unsymmetric composite plates. *Composites Science and Technology*, **63**, pp. 187–197 (2003).

[10] Timmerman J.F., Hayes B.S., SeferisJ.C. Cure temperature effects on cryogenic microcracking of polymeric composite materials. *Polymer Composites*, **24**, pp. 132–139 (2003).

[11] Shokrieh M.M., Kamali S.M. Theoretical and experimental studies on residual stresses in laminated polymer composites. *Journal of Composite Materials*, **39**, pp. 2213–2225 (2005).

[12] Maimí P., Camanho P.P., Mayugo J.A., Turon A. Matrix cracking and delamination in laminated composites. Part I: Ply constitutive law, first ply failure and onset of delamination. *Mechanics of Materials*, **43**, pp. 169–185 (2011).

[13] Hashin Z. Finite thermoelastic fracture criteria with application to laminate cracking analysis. *Journal of the Mechanics and Physics of Solids*, **44**, pp. 1129–1145 (1996).

[14] Machado R.D., Filho J.E.A., da Silva M.P. Stiffness loss of laminated composite plates with distributed damage by the modified local greens function method. *Composite Structures*, **84**, pp. 220–227 (2008).

[15] Joffe R., Varna J. Analytical modeling of stiffness reduction in symmetric and balanced laminates due to cracks in 90° layers. *Composites Science and Technology*, **59**, pp. 1641–1652 (1999).

[16] Varna J., Joffe R., Talreja R. A synergistic damage-mechanics analysis of transverse cracking in $[\pm\theta/90_4]_s$ laminates. *Composites Science and Technology*, **61**, pp. 657–665 (2001).

[17] Wang J., Karihaloo B.L. Optimum in situ strength design of composite laminates. Part I: In situ strength parameters. *Journal of Composite Materials*, **30**, pp. 1314–1337 (1996).